To appear in the Proceedings of the 2005 IEEE Aerospace Conference, Big Sky, MT, March 2005

The Mars Exploration Rover Instrument Positioning System

Eric T. Baumgartner, Robert G. Bonitz, Joseph P. Melko, Lori R. Shiraishi and P. Chris Leger
Jet Propulsion Laboratory
California Institute of Technology
4800 Oak Grove Drive
Pasadena, CA 91109-8099
Eric.T.Baumgartner,Robert.G.Bonitz,Joseph.P.Melko,Lori.R.Shiraishi,Chris.Leger@jpl.nasa.gov

Abstract—During Mars Exploration Rover (MER) surface operations, the scientific data gathered by the *in situ* instrument suite has been invaluable with respect to the discovery of a significant water history at Meridiani Planum and the hint of water processes at work in Gusev Crater. Specifically, the ability to perform precision manipulation from a mobile platform (i.e., mobile manipulation) has been a critical part of the successful operation of the Spirit and Opportunity rovers. As such, this paper[1,2] describes the MER Instrument Positioning System that allows the *in situ* instruments to operate and collect their important science data using a robust, dexterous robotic arm combined with visual target selection and autonomous software functions.

TABLE OF CONTENTS

1. INTRODUCTION

The Mars Exploration Rovers, Spirit and Opportunity, carry a unique *in situ* instrument suite that has been designed to measure and understand the detailed geochemistry and morphology of the surface of Mars [1]. The *in situ* instrument suite includes the Mössbauer Spectrometer (MB) [2], the Alpha Particle X-ray Spectrometer (APXS) [3], the Microscopic Imager (MI) [4], and the Rock Abrasion Tool (RAT) [5]. The deployment and placement of these instruments onto the Martian surface (both soil and rock targets) is controlled by the 5 degree-of-freedom Instrument Deployment Device (IDD). The IDD represents the most dexterous robotic manipulator ever flown to another lunar or planetary surface.

The IDD is mounted towards the front of the rover and is capable of reaching out approximately 0.75 meters in front of the rover at full extent. The IDD weighs approximately 4 kg and carries a 2 kg payload mass (instruments and associated structure). Certain aspects of the mechanical design of the IDD are described in [6,7]. During rover driving activities, the IDD is contained within a stowed volume that does not impact the rover's ability to traverse safely across the Martian terrain. The location of soil and rock targets which the scientists select for instrument placement activities are specified using the front Hazard avoidance cameras (or front Hazcams) which are configured as a stereo camera pair.

On-board software controls the IDD based on sequences developed by ground operators. The on-board software contains numerous low-level and high-level functions for controlling the IDD such as actuator current limiting based on temperature and pose, inverse kinematic Cartesian control, deflection compensation due to gravity and tilt-induced droop, model-based pre-loading of instruments on hard targets, instrument placement using proximity feedback sensors, etc. For the MER project, the entire scope of work associated with the design, development, test and operation of the IDD and *in situ* instruments was grouped into the Instrument Positioning System (IPS). As with many of the other rover sub-systems, the IPS was a collaborative effort between scientists, engineers, and instrument developers that culminated in the successful operation of this dexterous robot arm for collecting important science data.

This paper will first lay out a summary of the system requirements that drove the design of the overall IPS. An overview of the mechanical configuration and specific design considerations is given in Section 3. The paper will also detail the flight software functions and algorithms utilized to command and control the IDD in order to perform autonomous surface operations in Section 4. The IPS test program will also be described in Section 5 including results from sub-system calibration activities. Finally, in Section 6, specific results and experiences from the surface operations phase will be presented, in particular, those results that highlight the precision and robustness of this robotic instrument positioning system.

[1] 0-7803-8870-4/05/$20.00© 2005 IEEE
[2] IEEEAC paper #1178, Version 6, Updated December 20, 2004

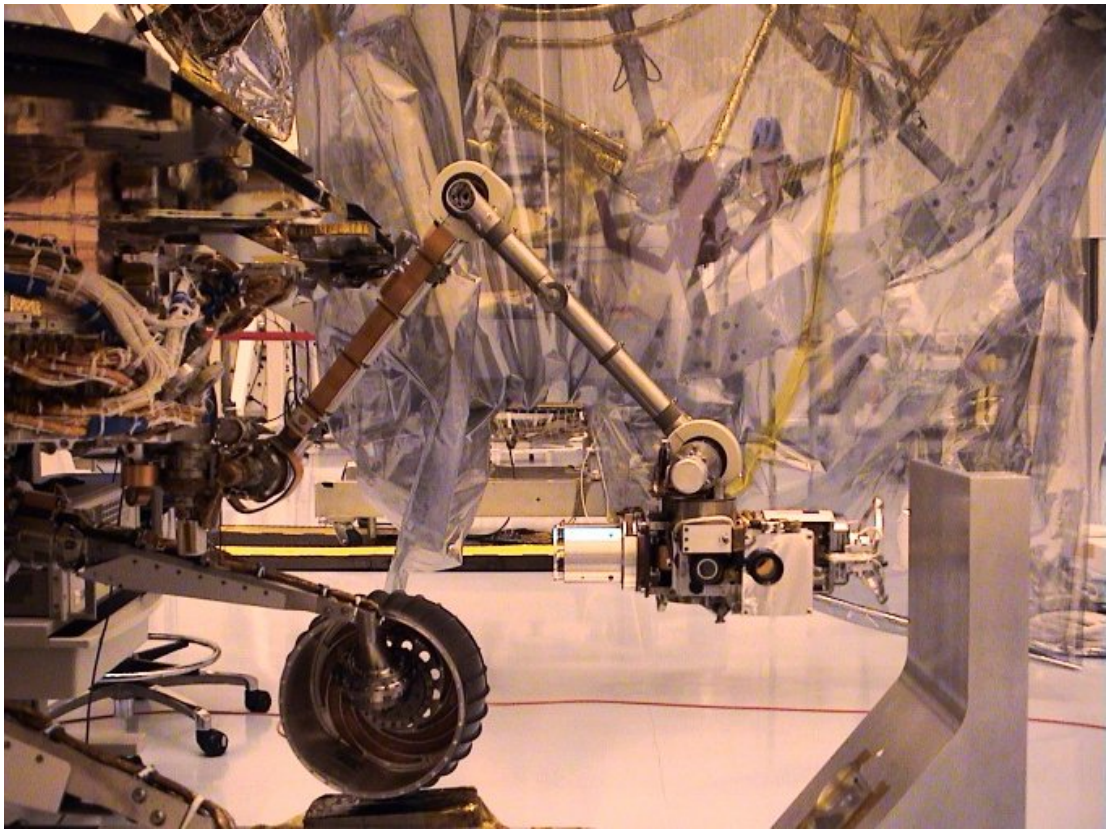

Figure 1: MER Instrument Positioning System

2. DRIVING SYSTEM REQUIREMENTS

The MER Instrument Positioning System is shown in Figure 1. The IPS includes the 5 degree-of-freedom (DOF) Instrument Deployment Device that is utilized to place and hold the *in situ* instruments on rock and soil targets located within the IDD work volume and the rover-mounted targets such as the dust collecting magnets and instrument calibration targets. The degrees-of-freedom of the IDD include five rotary actuators called the shoulder azimuth, shoulder elevation, elbow, wrist and turret. For placement of the instruments on rock and soil targets, a wide field-of-view stereo imaging system known as the front Hazcam is used to specify the 3D location and surface normal of the target with respect to the rover's coordinate frame. On-board software is then used to drive the IDD so that the selected instrument achieves the desired 3D position and 2D orientation (azimuth and elevation) relative to the target of interest. Proximity sensors are located on all instruments so that contact with the target surface can be detected and trigger the termination of the IDD movement.

The driving system requirements for the IPS are primarily concerned with the absolute and relative positioning performance associated with the placement of the instruments on targets of interest including rock and soil targets as well as rover-mounted targets. The absolute positioning requirement stated that the IPS shall be capable of positioning each *in situ* instruments to within 10 mm in position and 10 degrees with respect to the surface normal of a science target that has not been previously contacted by another *in situ* instrument. This requirement was then broken down into two error budgets associated with the ability of the IDD to achieve a certain instrument position and orientation and the ability of the front Hazcam stereo camera pair to resolve the 3D position and surface normal of a science target. Therefore, the overall absolute positioning and orientation error requirements were split equally into two error budgets.

The IDD was required to be capable of achieving a position accuracy of 5 mm and an angular accuracy of 5 degrees in free space within the dexterous workspace of the IDD. Factors that affect the ability of the IDD to meet this requirement include knowledge of the IDD kinematics (link lengths, link offsets, etc), knowledge of the location of actuator hardstops used to home the actuators, actuator backlash effects, closed-loop motion controller resolution, and knowledge of IDD stiffness parameters. A calibration procedure (to be described in Section 5) was utilized to experimentally determine the parameters that affect the IDD positioning performance. The remaining half of the error budget was assigned to the front Hazcam stereo pair such that the vision system was required to determine the location of the science target with a position accuracy of 5

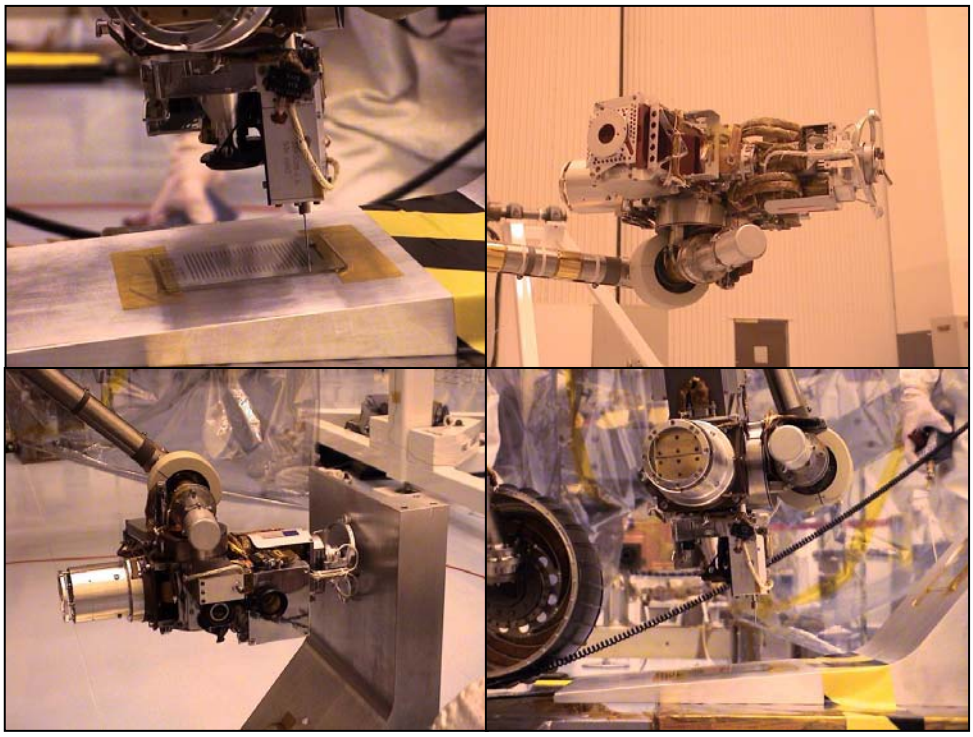

Figure 2: Instrument Proximity Sensors

mm and the angular accuracy was 5 degrees with respect to the target's surface normal. Factors that affect the ability of the stereo camera pair to meet this requirement include camera calibration errors, stereo correlation errors, and image resolution issues.

Another driving system requirement is associated the repeatability of the IDD in terms of being able to place one instrument on a science target after the target has been contacted by a different instrument, to place the instruments on rover-mounted targets, and to perform close-clearance operations such as stowing the IDD within its stowed location. The requirement specified that the repeatability of the IDD shall be 4 mm in position and 3 mm in orientation. The final positioning requirement is associated with the ability of the IDD to incrementally position the MI. The MI is a fixed focus instrument with a depth of field of 3 mm. Therefore, the IDD serves as the focus mechanism for the MI. As such, the IDD is required to have a minimum controllable motion of 2 mm ± 1 mm.

In addition to the positioning requirements mentioned above, other driving system requirements included the ability to place any *in situ* instrument on a reachable science target within one command cycle and to be able to remove an instrument from a target and place a second instrument on the same target any time during the Martian diurnal cycle (i.e., day or night). For RAT grinding operations, the IDD is required to place and hold the RAT on the rock target with a specified preload. The IDD is required to provide the RAT with a preload of at least 10N within 90% of the reachable science target workspace. As mentioned previously, each instrument carried proximity sensors to detect contact between the instrument and the target surface. For the MI, MB and RAT, the contact sensors are configured to be dual redundant per instrument. The APXS instrument includes an integral dust door mechanism whose operation is controlled by the IDD's placement of the APXS on a hard target (rover-mounted target or a rock target). The APXS dust door mechanism includes a latch switch that is used to sense the successful opening or closing of the dust door and a second (non-redundant) contact switch that is activated after the dust door has been latched open. The proximity sensing devices for each *in situ* instrument are shown in Figure 2.

3. MECHANICAL OVERVIEW

The mechanical design of the IDD proved to be quite challenging with respect to the allowable stowage volume for the IDD and the instruments. The volume for stow was approximately 500 x 296 x 178 mm. The diameter of the volume swept by spinning the turret assembly, which had to be wrapped into this space along with the arm, was 318 mm. The stowed volume is located below a shelf of the main rover body and, in order to allow activities in rough Martian terrain, the arm had to be designed to deploy without dropping below the belly pan of the rover. In addition, the swept volume of the rover's articulating mobility system (rocker-bogie suspension system) is located on both sides of the IDD volume. Finally, the mobility system, when stowed for launch, wraps tightly around the stowed volume

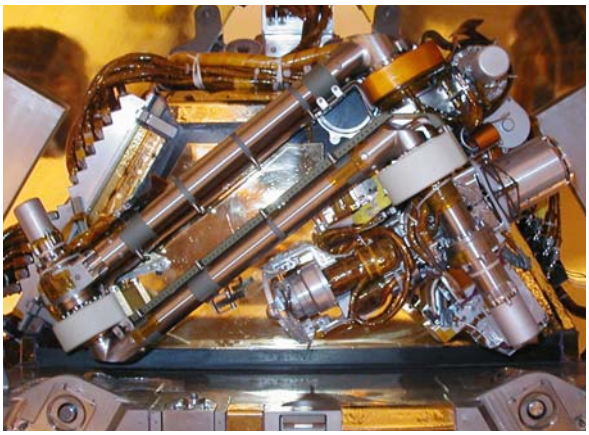

Figure 3: IDD in Stowed Configuration (view from below rover)

provided for the IDD. The stowed volume of the IDD is shown in Figure 3.

The mass allocation for the IDD of 4.4 kg, including launch restraints and cabling, was also an extreme design driver. The cabling mass alone, mostly to support instruments, was almost 1 kg. The arm had to support a turret of instruments with a mass of 2 kg, provide preload for the RAT, and be capable of achieving the absolute and repeatable positioning requirements described in Section 2.

The mass allocated and load magnifications possible with the 5 DOF robot arm did not allow the structure and joints to be designed in such a way that the arm could not damage itself in all possible operational cases. Instead, an approach which integrated flight software fault protection, operational constraints, and mechanical capability was developed that reduced the risk of damaging the IDD during normal operations. Joint flexibility became particularly important since arm configurations that cause dangerous load magnifications also allow for significant travel past the point of instrument contact before the loads reach their critical stage. A redundant method of terminating IDD motion based on contact sensor feedback and tight limits on over travel past the expected contact point keep the arm in the safe load zone. While the torque used to get the joints started is capable of creating unsafe loads, software quickly ramps the current limit down after movement starts before more movement occurs than arm flexibility can accommodate. Software also limits the torque of the motors when the arm is in configurations that can magnify loads.

Another difficult problem was associated with locking the IDD and instruments for survival during launch and landing loads with only 2 release devices as well as providing a means to restow the IDD during rover motion. The elbow was locked in 2 degrees-of-freedom by a simple pin puller. The turret was locked directly to the rover body in 6 degrees-of-freedom. The space available and need to isolate the instruments from a significant pyrotechnic shock resulted in a three part system. First, a cable cutter (a low shock pyrotechnic device) was used to release pins actuated by mechanical springs which served to release 4 degrees-of-freedom. The movement of the IDD's shoulder azimuth joint was then used to pull the turret off the last fixed pin which constrained the final 2 degrees-of-freedom.

The extremely tight mass allocation did not allow the joints of the arm to be sized to hold the instrument turret without backdriving the joints or causing damage to the gears or structure of the joints during loads induced while driving. Restow was accomplished by inserting a "T" sticking up from the turret into a flanged C-channel on the rover body and by placing the elbow on a hook. The fit between the "T" and channel is very loose, on the order of several millimeters, in order to allow for some inaccuracy in the turret position when inserting the T into the channel. During rover surface mobility, the flexibility of the arm joints ensure that the loads on the arm do not dramatically increase before the T hits the side of the channel and resists further motion. The IDD restow features are shown in Figure 4.

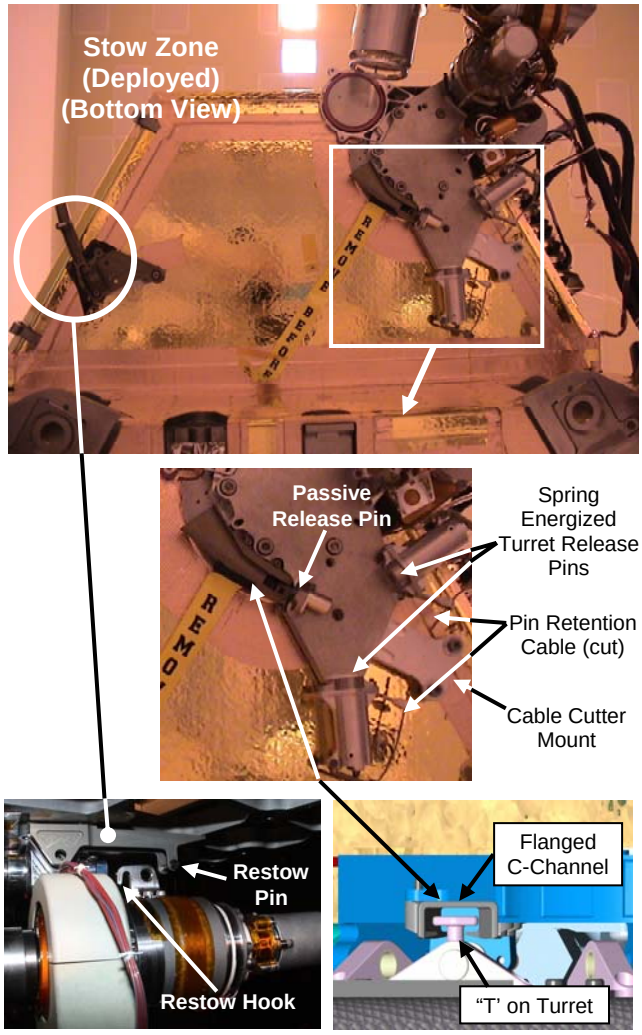

Figure 4: IDD Restow Features

The mechanisms used at each joint were optimized for mass, accuracy and space available for the mechanism and associated cable routing. Each joint was custom designed using various combinations of common components. All joints use DC motors with brushes that are optimized for operation within the Martian atmosphere along with a magneto resistive encoder mounted to the motor shaft. The encoder has 2 channels (for direction knowledge) and resolution is 128 counts per revolution. Counting encoder pulses from a known position such as launch stow or an actuator hard stop was the primary method of determining the position of each joint. A four position magnetic detent assembly was added to each motor to maintain joint position when power is turned off. In addition, the rover electronics enable dynamic braking by shorting the motor windings with a relay when the motor is not in use.

The mechanism gear trains all start with the same 3 stages of planetary gears attached to the motor. The shoulder and elbow joints add cup style, S-tooth harmonic drives to minimize backlash and mass. High loads at these joints required the use of a very mass efficient gear system. The wrist and turret joints use 2 additional stages of planetary gears. Using the planetary gears as the final stages in these joints was the result of a trade between the pros of mass, smaller package, less cost versus the cons of reduced absolute accuracy and repeatability. Also, the shorter distance between these joints and the end of the instruments somewhat mitigated the accuracy issues. As a representative example, the IDD elbow joint is shown in Figure 5.

Titanium (Ti) was used for the housings and shafts to best match the bearing, gear and motor contraction/expansion with temperature. Loose fits in the final gear stages or output ball bearings could not be tolerated due to the accuracy and repeatability requirements of the IDD. The links between joints were also Ti rather than composite due to concerns about bond integrity and load carrying ability in the end fittings at -105 degrees C after multiple thermal cycles.

Lubrication was a challenge due to the extremely cold temperatures at which the arm was required to move (-55 degrees C allowable, -70 degrees C qualification). These temperatures were slightly below the minimum operating range of any space rated wet lubrication. However, the rather low total travel (life) requirements indicated that the mechanism would last long enough with only a very small amount of lubricant. A process called grease plating was used to apply only a very thin coating of lubricant to all moving parts. For some components, extra grease was added just outside the wear tracks or extra drops of oil were added. While the lubricant begins to get very sticky at the low temperatures, this thin coating minimized by a factor of 2:1 the overall torque required to overcome lubrication drag between warm and cold temperatures. Additional torque capability was designed into the actuators to handle

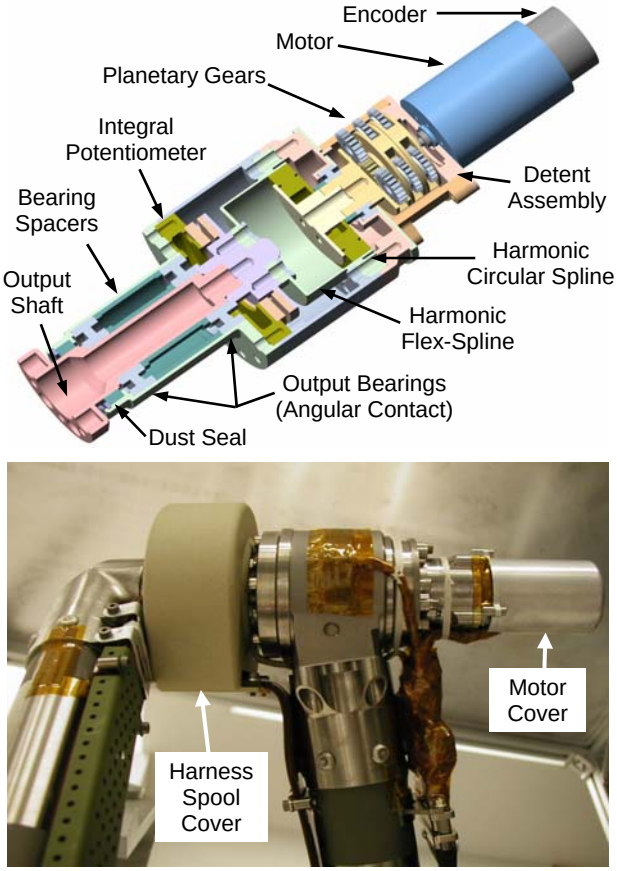

Figure 5: IDD Elbow Joint

lubrication drag. In addition, the flight software modifies the amount of current as a function of temperature in order to ensure that the extra capability needed for cold temperatures does not cause damage to the actuator when it is warmer.

All joints were sealed from external contaminants using spring energized, Teflon O-rings. Additional felt and labyrinth seals were used as extra protection for specific applications. Each joint has a rotary potentiometer for gross, absolute position estimation as a check on the position number generated from the relative encoders on the motors. In addition, if the encoder count was determined to be in error, the potentiometers were intended to provide enough data to get to the arm to safe positions to reset the encoder counts using the hard stops. The ratio of wiper voltage to excitation voltage is used in order to avoid inaccuracies caused by the large temperature range and the variance in bus voltage. The shoulder azimuth and elevation joints take advantage of their small travel range to improve accuracy by using a no-backlash speed increaser between the potentiometer and the output shaft. This method also reduced mass and eased packaging issues for these joints.

All joints have electric heaters which are utilized during night operations to raise the joint temperatures from -105 degrees C to the minimum operating temperature of -55

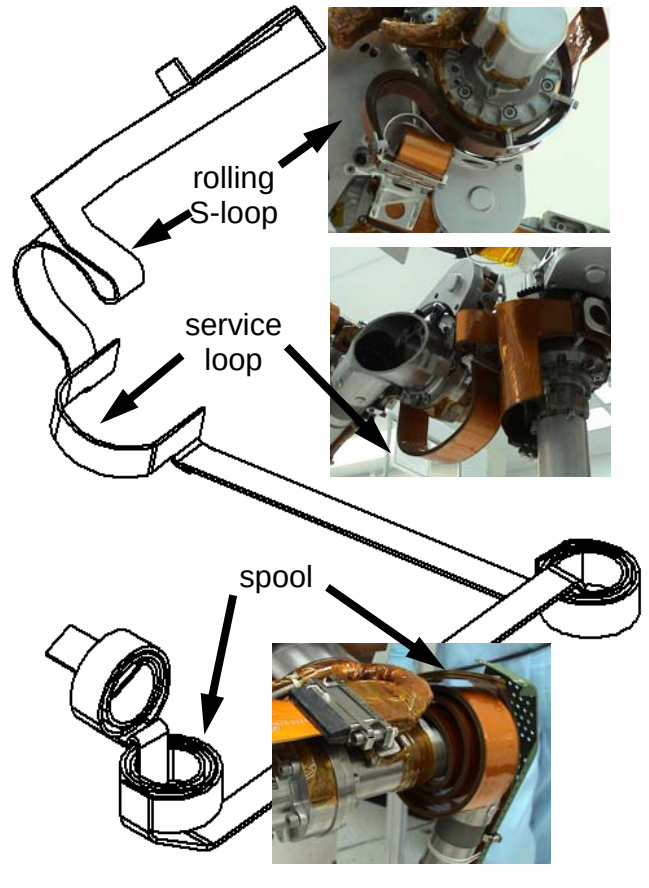

Figure 6: IDD Flex Cable Routing

degrees C. During surface operations, the required heating times are based on model-based thermal predictions. The shoulder azimuth joint and turret joint include thermistors to provide temperature telemetry and improvements to the model-based heating duration prediction algorithm. A thermostat on the rover platform disconnects the heaters when the atmospheric temperature rises to daytime temperatures to protect joints from being overheated if a heater is accidentally left on.

A cable harness of over 200 conductors is routed through the arm with some of the conductors terminating at the joint actuators, however, most conductors are carried all the way to the instrument turret at the end of the IDD. Strips of flat flexprint cabling were used where each strip consisted of 2 layers of conductor traces sandwiched between 2 thin conductive shield layers. The cables terminate in factory-installed micro-D connectors. To reduce mass, volume, risk and electrical noise, each flexprint cable runs continuously, with no intermediate connections, between the IDD connector bulkhead at the rover and the serviced component. Some cables branch into 2 half-wide strips midstream to reach separated components. Three different methods were used to route the cables across the rotating joints. The shape was also constrained by width and height maximums during initial fabrication in flat form. Cabling with the potential to be near the ground also had to be contained and protected. All of these requirements resulted in a very complex cable routing and custom shapes for each cable as shown in Figure 6. Due to the extra length needed for flexing across joints, the actual length of cable from the IDD/rover connector bulkhead to the instrument is approximately 3 meters. Much effort went into grouping conductors and shielding sensitive lines with extra shielding traces to minimize noise with line impedance being a significant design driver for some instruments. All of these cable issues had to be addressed at the system level as the entire cable route between the sensors and the electronics included up to 0.7 meters of round wire cabling which then entered another 1.3 meters of flat flexprint cabling before getting to the electronics boards located inside the rover.

Two of the instrument contact sensors (MI and MB) were custom designed to allow the arm to find the surface reliably in very dusty conditions and after several immersions in Martian soil. The contact sensor on the MB has a large footprint area to ensure it triggers on very soft objects while the MI contact sensor allows very accurate location assessment of very small points on a rock or hard surface. The contact sensors were designed to handle the expected abuse which comes with placement on uneven terrain. The MB contact sensor structure included feet under the contact sensor plate which lock onto the strong instrument end cap to prevent the sensor from being bent sideways in a glancing contact. The MI contact sensor uses a coiled spring at its base to allow it to be bent 90 degrees sideways with permanent damage. For the MI and MB, the actual electric switches are protected in housings and are protected from any loads by the parallel flexure assembly which holds the external contact parts as shown in Figure 7. The flexures allow surface detection at very low loads. For debris tolerance, pivoting parts have been kept to a minimum and there are no sliding parts anywhere in the assembly other than the felt seal used to minimize dust entering the housing.

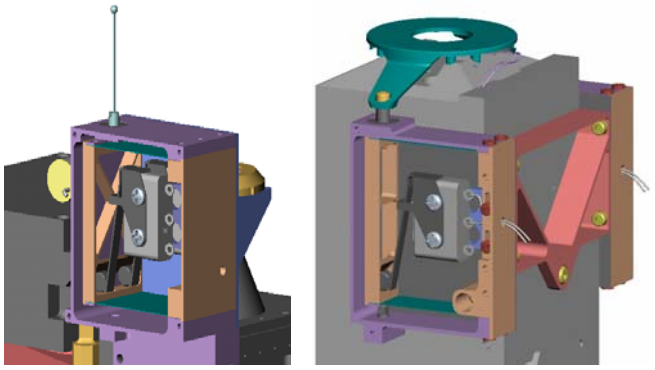

Figure 7: MI and MB Contact Sensor Hardware

4. ALGORITHMS AND SOFTWARE

Overview

Control of the IDD is accomplished through a distributed architecture with the necessary functions implemented in various hardware and flight software (FSW) modules as depicted in Figure 8. Low-level PID control of the IDD motors and generation of trapezoidal velocity profiles are implemented in hardware on the Motor Control Board (MCB) using feedback from quadrature encoders on the motor shafts. The motor controller runs at a sampling frequency of 1KHz. The states of the joint potentiometers, temperature sensors, and contact switches (CSWs) are scanned by the Payload Services Analog Board (PSAB) and converted to digital format for processing by the flight software. The states of the contact switches are also fed directly to the hardware motor controller so that motion can be terminated if so desired upon change of a switch state.

The FSW resides on the Command and Data Handling (C&DH) computer (a RAD6000) located in a VME chassis within the rover's electronics box. The FSW runs under VxWorks[3], a real-time multi-tasking operating system with selectable task priorities and preemptive rescheduling. The primary method of communication between tasks is via message passing. A high-level view of the IDD software module is depicted in Figure 9. The IDD task waits until a message is received and then responds to the message. After completing the response, it waits for the next message. The message can be a command, and out-of-bounds (OOB) message (e.g., stop), or a reply from the motor (MOT) software containing the state of the IDD motors and sensors. The IDD software also provides a function for other software modules to get the IDD state information for inclusion in instrument (APXS, MB, MI, RAT) data products to make correlation of IDD state with the science data easy to accomplish during ground data processing.

A simplified view of the sequence of events when the IDD

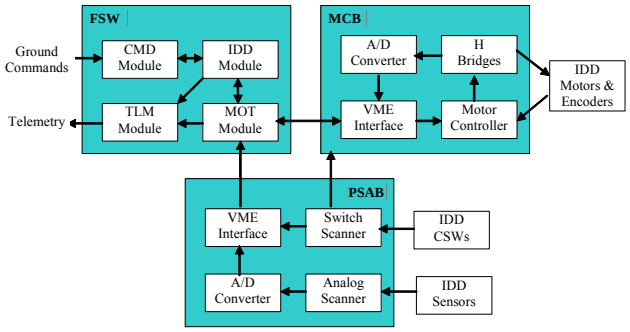

Figure 8: IDD Control Architecture

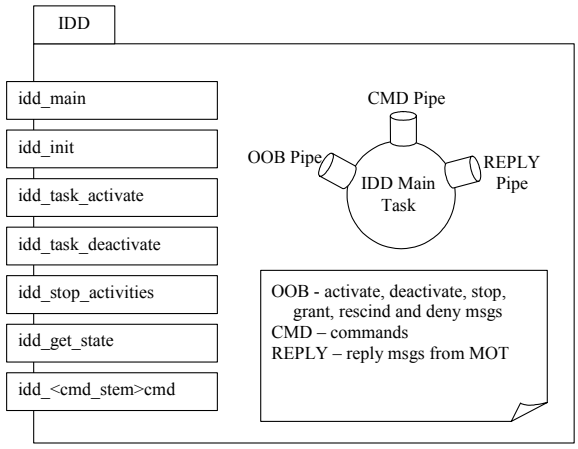

Figure 9: IDD Software Overview

software receives a command is depicted in Figure 10. Prior to actually moving the arm the IDD must get permission from the Activity Constraint Manager (ACM) and the Arbiter (ARB) to assure that it is safe to move the arm (e.g., not driving, no faults) and that the necessary resources are available (the motor controller is shared with other rover mechanisms). At the completion of the move, the resources are released and the IDD FSW replies to the command object that the command completed – successfully or not.

Kinematics

The IDD kinematics are defined using the Denavit-Hartenberg [8] representation with the coordinate frames assigned as shown in Figure 11 and summarized in Table 1. The z axis for each instrument frame is aligned with its "boresight." To eliminate joint angles that are congruent modulo 2π, each is uniquely expressed as a negative number from the joint's negative hardstop, $\theta_{\min_i}$, to zero and as a positive number from zero to the joint's positive

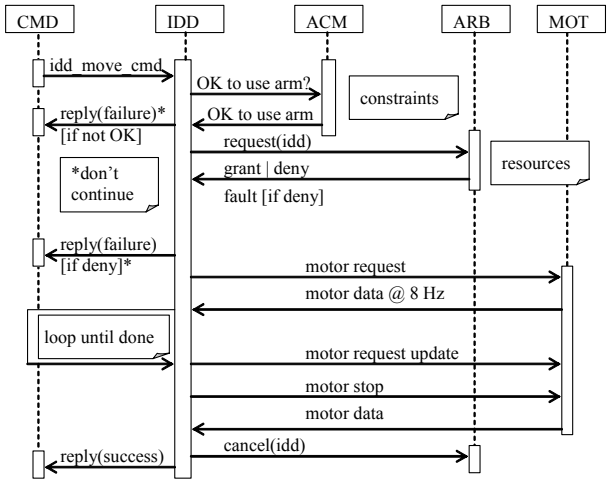

Figure 10: IDD Command Sequence Diagram

[3] VxWorks is registered trademark of Wind River Systems, Inc., 1010, Atlantic Avenue, Alameda, CA 94501

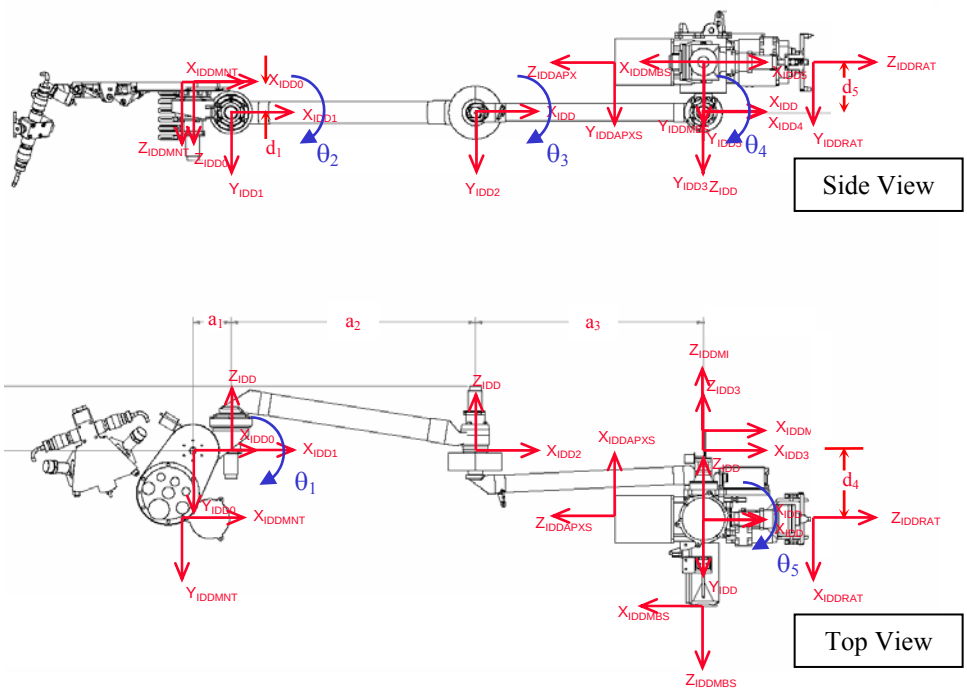

Figure 11: IDD Mechanical Layout and Coordinate Frame Conventions

hardstop, $\theta_{\max_i}$. The following link and joint parameters are defined:

a_i = i^{th} link length = distance along x_i from the intersection of the x_i and z_{i-1} axes to the origin of the i^{th} frame;

d_i = i^{th} offset = distance along z_{i-1} from origin$_{i-1}$ to the intersection of the x_i and z_{i-1} axes;

ϕ_i = i^{th} twist = angle from z_{i-1} to z_i about x_i;

θ_i = i^{th} joint variable; the angle from x_{i-1} to x_i about z_{i-1}.

The following kinematic variables are defined:

- Position: the x, y, and z coordinates of the origin of the tool frame in the rover frame.
- Orientation: the direction of the tool frame approach vector (z axis) as specified by the azimuth and elevation angles, θ_{az} and θ_{el}. Since the IDD has only 5 DOF, the orientation about the approach vector is not controlled.
- θ_{az}: the angle from the rover $+x$ axis to the projection of the tool approach vector onto the rover x-y plane with the positive sense being about the rover $+z$ axis using the right-hand rule. The rover $+x$ axis points forward and the $+z$ axis point down.
- θ_{el}: the angle from the projection of the tool approach vector onto the rover x-y plane to the approach vector with the positive sense having the approach vector z coordinate greater than 0 for a positive angle.

Link	a_i	ϕ_i	d_i	θ_i
1	a_1	$\pi/2$	d_1	θ_1
2	a_2	0	0	θ_2
3	a_3	0	0	θ_3
4	0	$-\pi/2$	d_4	θ_4
5	0	$\pi/2$	d_5	θ_5

Table 1: IDD Kinematic Parameters

- Pose = $[x \quad y \quad z \quad \theta_{az} \quad \theta_{el}]^T$: the Cartesian position and orientation of the designated instrument or tool frame (MB, APXS, RAT, MI) in the rover coordinate frame. Tool frames are located at the face of the instrument with the approach vector (z axis) along the "boresight."
- Configuration: the geometric state of the shoulder, elbow and wrist. The shoulder can take on two values – RIGHT (1) or LEFT (-1), the elbow two values – UP (1) or DOWN (-1), and the wrist two values – UP (1) or DOWN (-1).
- ${}^iT_j = \begin{bmatrix} {}^iR_j & {}^ip_j \\ 0\ 0\ 0 & 1 \end{bmatrix}$: the homogeneous transformation from frame i to j;
- ${}^iR_j = \left[{}^in_j \ {}^is_j \ {}^ia_j \right]$: the orientation of frame j in frame i;

- ${}^{i}a_{j}$: the unit vector of the *z* axis of frame *j* in frame *i*;
- ${}^{i}p_{j}$: the vector from the origin of frame *i* to the origin of frame *j*.

Symbols used in the kinematic equations are:

$s_i = \sin(\theta_i)$;
$c_i = \cos(\theta_i)$;
$s_{ijk} = \sin(\theta_i+\theta_j+\theta_k)$;
$c_{ijk} = \cos(\theta_i+\theta_j+\theta_k)$.

The pose is computed from the joint angles by first computing the homogeneous transformation from the rover frame to the tool frame:

$$ {}^{rover}T_{tool} = {}^{rover}T_{IDDmnt}\,{}^{IDDmnt}T_{IDD0}\,{}^{IDD0}T_{IDD5}\,{}^{IDD5}T_{tool} \tag{1}$$

where

$$ {}^{IDD0}T_{IDD5} = \begin{bmatrix} c_1c_{234}c_5 - s_1s_5 & -c_1s_{234} & c_1c_{234}s_5 + s_1c_5 & a_1c_1 + a_2c_1c_2 + a_3c_1c_{23} + d_4s_1 - d_5c_1s_{234} \\ s_1c_{234}c_5 + c_1s_5 & -s_1s_{234} & s_1c_{234}s_5 - c_1c_5 & a_1s_1 + a_2s_1c_2 + a_3s_1c_{23} - d_4c_1 - d_5s_1s_{234} \\ s_{234}c_5 & c_{234} & s_{234}s_5 & d_1 + a_2s_2 + a_3s_{23} + d_5c_{234} \\ 0 & 0 & 0 & 1 \end{bmatrix} \tag{2}$$

and

$$ {}^{IDD5}T_{IDDtool} = \begin{bmatrix} c_{tool} & 0 & s_{tool} & {}^{5}p_{toolx} \\ 0 & 1 & 0 & 0 \\ -s_{tool} & 0 & c_{tool} & {}^{5}p_{toolz} \\ 0 & 0 & 0 & 1 \end{bmatrix} \tag{3}$$

and then computing the pose from:

$$ pose = \left[{}^{rover}p_{tool}^{T} \quad \arctan 2({}^{rover}a_{tooly}, {}^{rover}a_{toolx}) \quad \arctan 2\left({}^{rover}a_{toolz}, \sqrt{{}^{rover}a_{tooly}^2 + {}^{rover}a_{toolx}^2} \right) \right]^{\mathrm{T}} \tag{4}$$

The configuration of the IDD is computed from:

$$ shoulder = \begin{cases} RIGHT & ;\ c_1\,{}^{IDD0}p_{IDD5x} + s_1\,{}^{IDD0}p_{IDD5y} \geq 0 \\ LEFT & ;\ c_1\,{}^{IDD0}p_{IDD5x} + s_1\,{}^{IDD0}p_{IDD5y} < 0 \end{cases} \tag{5}$$

$$ elbow = \begin{cases} UP & ;\ shoulder = RIGHT\ \&\ {}^{IDD2}p_{IDD3y} \geq 0 \\ & ;\ shoulder = LEFT\ \&\ {}^{IDD2}p_{IDD3y} \leq 0 \\ DOWN & ;\ shoulder = RIGHT\ \&\ {}^{IDD2}p_{IDD3y} < 0 \\ & ;\ shoulder = LEFT\ \&\ {}^{IDD2}p_{IDD3y} > 0 \end{cases} \tag{6}$$

$$ wrist = \begin{cases} UP & ;\ {}^{IDD0}a_{4z} \geq 0 \\ DOWN & ;\ {}^{IDD0}a_{4z} < 0 \end{cases}. \tag{8}$$

The inverse kinematics were derived using geometric techniques and is computed as described below.

First compute the approach vector in the rover frame from the desired instrument azimuth and elevation angles:

$$ {}^{rover}a_{tool} = \begin{bmatrix} c_{el}c_{az} & c_{el}s_{az} & s_{el} \end{bmatrix}^{T}. \tag{7}$$

Compute the position of the turret frame in the IDD base frame:

$$ {}^{IDD0}p_{IDD5} = {}^{IDD0}p_{tool} - {}^{IDD0}a_{tool} \left\| {}^{5}p_{tool} \right\|. \tag{8}$$

Then compute the joint angles:

$$ \theta_1 = \begin{cases} \alpha_1 + \beta_1 & ;\ shoulder = RIGHT \\ \alpha_1 - \beta_1 - \pi & ;\ shoulder = LEFT \end{cases} \tag{9}$$

where

$$ \alpha_1 = \arctan 2\left({}^{IDD0}p_{IDD5y},\ {}^{IDD0}p_{IDD5x} \right) \tag{10}$$

$$ \beta_1 = \arctan 2\left(d_4, \sqrt{{}^{IDD0}p_{IDD5x}^2 + {}^{IDD0}p_{IDD\%y}^2 - d_4^2} \right) \tag{11}$$

$$ \theta_2 = \alpha_2 - shoulder \times elbow \times \beta_2 \tag{12}$$

where

$$ \alpha_2 = \arctan 2\left({}^{IDD1}p_{IDD4y},\ {}^{IDD1}p_{IDD4x} \right) \tag{13}$$

$$ r_3 = \sqrt{{}^{IDD1}p_{IDD4x}^2 + {}^{IDD1}p_{IDD4y}^2} \tag{14}$$

$$ \beta_2 = \arccos\left(\frac{r_3^2 + a_2^2 - a_3^2}{2r_3a_2} \right) \tag{15}$$

$$ \theta_3 = \arctan 2\left(shoulder \times elbow \times s_3,\ c_3 \right) \tag{16}$$

where

$$ c_3 = \frac{r_3^2 - a_2^2 - a_3^2}{2a_2a_3} \tag{17}$$

$$ s_3 = \sqrt{1 - c_3^2} \tag{18}$$

$$ \theta_4 = \theta_{234} - \theta_2 - \theta_3 \tag{19}$$

where

$$ \theta_{234} = \arctan 2\left({}^{IDD0}a_{toolz},\ c_1\,{}^{IDD0}a_{toolx} + s_1\,{}^{IDD0}a_{tooly} \right) \tag{20}$$

$$ \theta_5 = \arctan 2\left(\begin{matrix} c_1c_{234}\,{}^{IDD0}a_{toolx} + s_1c_{234}\,{}^{IDD0}a_{tooly} + s_{234}\,{}^{IDD0}a_{toolz}, \\ s_1\,{}^{IDD0}a_{toolx} - c_1\,{}^{IDD0}a_{tooly} \end{matrix} \right) - \theta_{tool} \tag{21}$$

Cartesian Trajectory Generation

When the IDD FSW receives a Cartesian move command, a sequence of intermediate or via points between the starting and ending poses is generated prior to the initiation of motion. The number of via points generated satisfies the following conditions: 1) the deviation from the Cartesian straight-line path is less than the specified error bound, ε_p, and 2) the Cartesian distance between via points is less the specified allowable distance, δ_p. The concept is illustrated in Figure 12. A corresponding set of conditions is also satisfied for orientation with the error bound and distance designated as, ε_o, and δ_o, respectively. Finally, the distance in joint space between the via points must be less than the specified allowable distance, δ_q. The distance and error bounds are be stored in the parameter table and can be changed by the operator, but a hard-coded lower limit is enforced under which the operator cannot set the limits.

The change in orientation from the starting to ending poses is represented as a change in the azimuth and elevation angles, θ_{az} and θ_{el}. Since θ_{az} and θ_{el} uniquely determine the approach vector of the designated tool, the change in orientation from the starting to ending poses can also be represented by a change in the starting and ending approach vectors. The ending approach vector can be obtained by rotating the starting approach vector about the common normal between the starting and ending approach vectors by an angle, θ_{n_c}. The "straight-line" orientation path is defined as a linear interpolation of θ_{n_c} about the common normal and is used in the generation of the via sequence.

The via sequence is generated using a recursive bisection method [9] and converted to a joint via sequence using the inverse kinematics described above for each of the Cartesian via points. Prior to initiation of motion, each via point is checked for joint limit violations and collisions with the rover. Trapezoidal velocity profiles are generated in hardware on the MCB such that all joints arrive at their via points simultaneously. The IDD FSW processes the position data during motion at an 8 Hz rate and when the arm is close to reaching a via point, the registers in the MCB are updated to the next set of joint via points. The hardware velocity profiler automatically generates the trapezoidal profile to the next via point on the fly so that smooth motion through each via point is achieved.

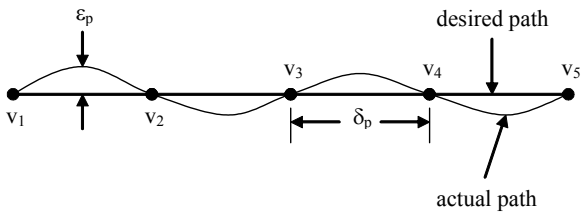

Figure 12: Cartesian Path Via Sequence

Deflection Compensation

The computation of the pose of the end effector from the joint angles using the forward kinematics function assumes that the IDD is rigid (i.e., infinitely stiff). However, the IDD's stiffness and mass properties are such that the endpoint can deflect significantly from the computed pose due to gravity. The deflection is also dependent on the tilt of the rover that affects the direction of the gravity vector relative to the IDD. In order to achieve the required placement accuracy, the commanded pose is adjusted based on the computed deflection. It is the adjusted pose that is used as the ending pose in the generation of the Cartesian via sequence described above. The computation is based on the stiffness model of the IDD and the mass properties of it and the instruments on the end effector. The deflection is dependent on the force exerted on the end effector and is used to compute the pose required to achieve a specified preload force on an instrument (e.g., RAT) when placed on a hard target.

The following parameters are defined for the deflection compensation algorithm:

m_i = lumped mass for the i^{th} link (all elements between i^{th}-1 frame and the i^{th} frame)

${}^{i-1}p_{cm_i}$ = vector from the i^{th}-1 coordinate frame to the i^{th} center of mass when θ_i is zero

$K_i = \begin{bmatrix} k_{ix} & 0 & 0 \\ 0 & k_{iy} & 0 \\ 0 & 0 & k_{iz} \end{bmatrix}$ = torsional stiffness matrix at the i^{th} frame

a_g = acceleration due to gravity.

The following variables are used in the algorithm:

${}^{i-1}R_{cm_i} = \begin{bmatrix} c_i & -s_i & 0 \\ s_i & c_i & 0 \\ 0 & 0 & 1 \end{bmatrix}$ = matrix representing rotation about the i^{th} joint axis

${}^{i-1}T_{cm_i} = \begin{bmatrix} {}^{i-1}R_{cm_i} & {}^{i-1}R_{cm_i}\,{}^{i-1}p_{cm_i} \\ 0\ 0\ 0 & 1 \end{bmatrix}$ = homogeneous transformation from (i-1) frame to the i^{th} center of mass

g_i = unit gravity vector at the i^{th} center of mass in the i^{th} center of mass frame

f_{end} = the force exerted along the tool frame z axis (approach vector)

$F_i = \begin{bmatrix} f_i^T & \tau_i^T \end{bmatrix}^T$ = the force and moment at the i^{th} frame in i^{th} frame coordinates

$\hat{p} = p\times = \begin{bmatrix} 0 & -p_z & p_y \\ p_z & 0 & -p_x \\ -p_y & p_x & 0 \end{bmatrix}$ = skew-symmetric cross-product operator for $p \in R^3$

${}^{i}Ad_j = \begin{bmatrix} {}^{i}R_j & {}^{i}\hat{p}_j\,{}^{i}R_j \\ 0_3 & {}^{i}R_j \end{bmatrix}$ = adjoint transformation which transforms twists from the i^{th} frame to the j^{th} frame where 0_3 is the 3x3 zero matrix

${}^{i}Ad_j^T = \begin{bmatrix} {}^{i}R_j^T & 0_3 \\ -{}^{i}R_j^T\,{}^{i}\hat{p}_j & {}^{i}R_j^T \end{bmatrix}$ = transpose of the adjoint transformation which transforms the force and moment acting at the i^{th} frame to the force and moment acting at the j^{th} frame.

Given the joint angles, the tilt, and the force exerted by the end effector, the deflected pose is computed as follows:

1. Compute the homogeneous transformations from the rover frame to the tool frame forward kinematics;
2. Compute the i^{th} gravity vector:
   g_{rvr} = gravity vector in the rover frame
   for i = 1 to 5:
   $g_i = {}^{i-1}R_{cm_i}^T\,{}^{rvr}R_{i-1}^T g_{rvr}$; (22)
3. Compute the force and moment vectors at i^{th} frame:
   $F_6 = F_{tool} = [0\,0\;\; -f_{end}\;\; 0\,0\,0]^T$ (23)
   for i = 5 to 0:
   $F_i = {}^{i+1}Ad_i^T F_{i+1} + {}^{cm_i}Ad_i^T \left[m_i a_g g_i^T\;\; 0\,0\,0\right]^T$; (24)
4. Compute the deflection and corresponding rotation matrix at the i^{th} frame:
   for i = 0 to 4:
   $d_i = {}^{i}R_{cm_i}^T (K_i^{-1})^{i}R_{cm_i}\tau_i$ (25)
   ${}^{i}R_d = aa2r\left(d_i, \|d_i\|\right)$ (26)
   where *aa2r* transforms the axis-angle representation of the deflection, d_i, to a rotation matrix in *SO(3)*;
5. Compute the i^{th} deflected homogeneous transformation:
   for i = 0 to 4:
   ${}^{i}T_{i+1} = \begin{bmatrix} {}^{i}R_d\,{}^{i}R_{i+1} & {}^{i}R_d\,{}^{i}p_{i+1} \\ 0\;\;0\;\;0 & 1 \end{bmatrix}$; (27)
6. Compute the deflected pose using the forward kinematics with the deflected homogeneous transformations.

Given a commanded pose, the tilt, and the force exerted by the end effector, the modified commanded pose is computed as follows:

1. Compute the joint angles, q_{cmd}, associated with the command pose using the inverse kinematics;
2. Compute the commanded homogeneous transformation, ${}^{rvr}T_{cmd}$, using the forward kinematics;
3. Compute the deflected homogeneous transformation, ${}^{rvr}T_d$, using the deflection computation algorithm of described above with q_{cmd} as the joint angles;
4. Compute the modified commanded homogeneous transformation:

$$ {}^{rvr}\tilde{T}_{cmd} = {}^{rvr}T_{cmd}\,{}^{rvr}T_d^{-1}\,{}^{rvr}T_{cmd} = \begin{bmatrix} {}^{rvr}R_{cmd}\,{}^{rvr}R_d^T\,{}^{rvr}R_{cmd} & {}^{rvr}R_{cmd}\,{}^{rvr}R_d^T\left({}^{rvr}p_{cmd} - {}^{rvr}p_d\right) + {}^{rvr}p_{cmd} \\ 0\;\;0\;\;0 & 1 \end{bmatrix} \quad (28) $$

The above transforms the commanded transformation to the modified transformation using the inverse of the computed deflection that is sufficiently accurate for small deflections.

Fault Protection

The IDD FSW monitors the state of the arm and rover prior to and during motion to assess if it is safe to continue or if any faults have occurred. The following types of faults are monitored:

- Trajectory generation error
- Potential collision
- Joint limit violation
- Out-of-envelope error
- Encoder-potentiometer miscompare
- Unexpected contact
- Unexpected motor stall
- Motor over heat
- Motor over current
- Excessive rover tilt
- Excessive change in rover tilt
- Requested preload will exceed structural limits

Motor currents are monitored to prevent excessive joint torques in the event that inadvertent contact of the arm or end effector occurs with the rover or an object in the environment. The current limits are computed based on the pose of the arm at each via point and the temperature. The pose-dependent portion of the current limit is computed using the deflection algorithm described above to get the joint toques necessary to statically hold the arm in position and additional amount to account for dynamic effects.

The temperature-dependent portion of the current limit is represented as the no-load motor current. Each joint was characterized for no-load current over temperature and speed. The no-load current is computed from:

$$ i_{nl} = c_0 + c_1 e^{c_2 T} + c_3 \omega e^{c_4 T} \quad (29) $$

where

c_i = constants derived by fitting to the data
T = temperature
ω = motor speed.

In addition to the running current limits, the joints require higher current at startup to overcome static friction. They are set higher at startup and then reduced on the fly once motion has begun.

Instrument Placement Behavior

During motion the IDD exhibits different behaviors depending on the operation being performed. The behaviors describe how the IDD responds to changes in conditions of contact sensors and joint motors. The IDD exhibits four basic behaviors during motion that are selectable by the operator:

- Free space – no contact is expected and any sense of contact from the contact switches is considered a fault.
- Guarded – contact by the current instrument on the target is expected and IDD motion stops when contact is detected. If the move is a Cartesian move, the pose is saved for future use by the change tool command that positions another instrument on the same target.
- Retracting – the instrument is removed from the target. In this behavior, contact switches for the selected instrument are masked during the move.
- Preload – the instrument is already in contact with the target during this behavior and the contact switches for the selected instrument are masked during the move. During a preload move, the instrument doesn't actually move since it is already in contact and the desired force is accomplished using the stiffness of the arm as described above in the deflection compensation algorithm.

Collision Checking

IDD collision checking is performed prior to initiation of motion at each via point along Cartesian and joint-space trajectories. The IDD collision checking software is based on the FIDO rover's collision checking software, described in [10]. Collision checking is performed by determining whether or not a geometric model of the rover arm intersects a geometric model of the rover. These geometric models are based on Oriented Bounding Boxes (OBBs) [11] and Oriented Bounding Prisms (OBPs), and are arranged hierarchically to reduce the total number of object-object intersection tests required to determine if an IDD pose is free of collisions. OBBs and OBPs offer a good trade-off of speed and accuracy: no divisions, transcendental operations, or iterations are required to determine if two OBBs or OBPs overlap, which leads to an extremely fast and robust implementation. OBBs and OBPs can tightly and efficiently bound the IDD geometry in a small number of primitives.

The collision checking software allows object and hierarchy definitions to be modified without recompilation so that changes can be made via commands sent to the rover. The IDD and rover are represented geometrically as a collection

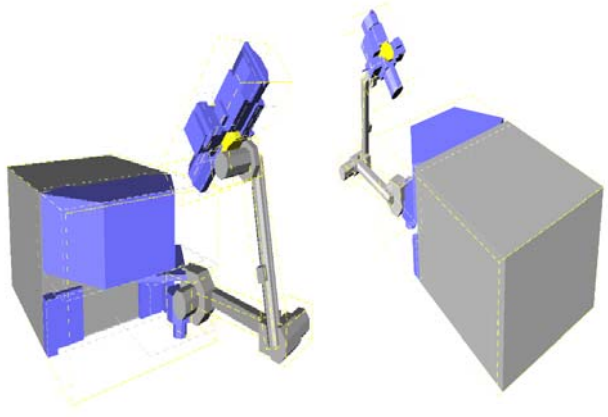

Figure 13: Partial OOB/OBP Models

of OBBs and OBPs attached to the coordinate system of each link. Each OBB/OBP is stored as an IDD collision object structure in a global list.

The current pose of each link is computing using the forward kinematic equations for the IDD, along with the predicted IDD deflection at each joint. If substantial deflection is expected within some links (as opposed to bearing slop at the joints), then the OBPs associated with the links will be expanded to account for the maximum deflected volume of the links. Object poses are defined relative to link coordinates, and the world-space object poses are computed by concatenating the relative pose to the pose of the link with which the object is associated.

The MER collision model is composed of a three-level hierarchy of OBPs and OBBs, with tight-fitting OBBs/OBPs for link geometry at the lowest level being contained within larger, less-accurate OBBs/OBPs at a higher level. The depth of the hierarchy is fixed at compile time. Only those objects that are leaves (i.e. have no child objects) actually represent the rover's geometry; the rest are containers that reduce the total number of object-to-object intersection tests. In addition to the IDD, the rover objects, solar panels, rockers, and front wheels are also modeled as a hierarchical collection of OBBs/OBPs. Figure 13 shows a portion of the OBB/OBP model for the collision checking software. The dashed boxes are container objects, while solid objects are lower level primitives directly representing rover geometry. The hierarchy level of each object is represented by color: yellow is highest, then grey, then blue. Each link has an independent hierarchy of objects.

5. SUB-SYSTEM CALIBRATION

Parameter Estimation

The primary sub-system calibration of the IDD consisted of "learning" the unique set of D-H parameters documented in Table 1, the joint position offsets, and the stiffness parameters described in Section 4. This was accomplished

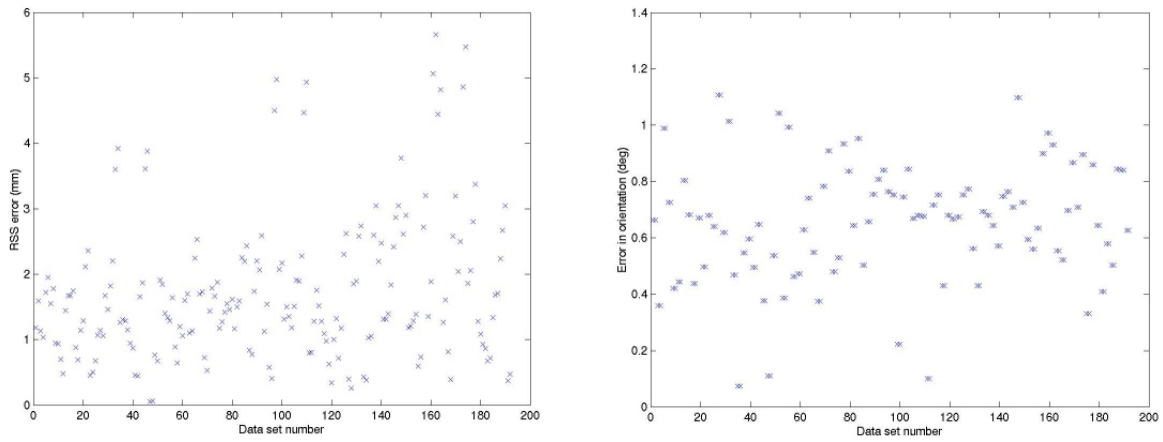

Figure 14: RSS position and orientation error for Spirit's IDD

by making use a precision measurement device known as a laser tracker to determine the 3D position of targets mounted to the end of the IDD as the robotic arm was moved throughout its workspace. A total of 2 laser tracker target brackets were mounted to test fixtures attached to the APXS and RAT mounting locations on the IDD turret. Each laser tracker target bracket was capable accepting 2 laser tracker targets. At unique IDD poses, the 3D location of two of the four targets was measured and the joint angles associated with the IDD pose were recorded within an IDD data product. Using the collected data sets, the parameters are computed using the parameter estimation technique that minimizes the least-squared error between the measured 3D position of the laser tracker targets and the computed 3D position of the laser tracker target using the deflected kinematics of the IDD.

For the Spirit rover, the data collection consisted of moving the IDD through a total of 96 poses in three distinct turret and IDD configurations and measuring the 3D position of two of the four laser tracker targets resulting in a total of 192 data points. The first configuration consisted of the IDD in a level configuration and the just the two laser tracker brackets mounted to the turret. The second configuration had the IDD in a level configuration with two laser tracker brackets mounted to the turret along with mass models mounted to the MB and MI mounting locations of the turret. In this configuration, the total mass of the laser tracker targets and the mass models simulated the full mass and center of mass of the *in situ* instruments as configured on the turret. The third configuration utilized the same turret configuration as the second configuration (laser tracker brackets and mass models) and tilting the IDD and associated ground support hardware by approximately 20 degrees. Finally, a "truth" data set was collected by moving the IDD through a different set of 30 poses in the third configuration. This truth set was not included in the least-squared error estimation process and was used to validate the parameters determined by this estimation process.

The position and orientation error residuals associated with the Spirit IDD training set are shown in Figure 14. The calibrated kinematic and stiffness parameters when compared to the nominal parameters that are derived from the CAD and finite element models of the IDD are shown in Table 2. The mean root sum squared (RSS) error associated with the Spirit IDD training set is 1.717 mm in position and 0.655 degrees in orientation. The mean plus 3σ RSS error for the Spirit IDD is 4.970 mm in position and 1.276 degrees in orientation. For the truth set, the mean RSS error is 2.081 mm in position and 0.677 degrees in position with the mean plus 3σ RSS error of 5.807 mm in position and 1.347 degrees in orientation. These RSS error number should be compared to the IDD positioning and orientation requirements described in Section 2 which specified a requirement of 5 mm in position and 5 degrees in orientation. Clearly, the Spirit IDD positioning and orientation performance exceeds the stated requirements.

For the Opportunity rover, the IDD calibration data collection process was similar to the Spirit rover with the exception of the inclusion of the third tilted configuration in the calibration data set. The data collection therefore consisted of 60 poses total and a total of 120 data points. The position and orientation residuals associated with the Opportunity IDD training set are similar to the Spirit data shown in Figure 14. The calibrated kinematic and stiffness parameters are also shown in Table 2 along with the Spirit and nominal parameter values. The mean RSS error associated with the Opportunity IDD training set is 1.024 mm in position and 0.452 degrees in orientation with the mean plus 3σ RSS error of 3.220 mm in position and 1.128 degrees in orientation. The truth set data consisted of 30 poses and resulted in a mean RSS error of 1.331 mm in position and 0.482 degrees in orientation with a mean plus 3σ RSS error of 3.560 mm in position and 1.202 degrees in orientation.

Parameters	Nominal	Spirit IDD	Opportunity IDD
(a_1, a_2, a_3) (meters)	(0.062, 0.354, 0.331)	(0.064, 0.353, 0.330)	(0.062, 0.354, 0.330)
(d_1, d_4, d_5) (meters)	(0.048, -0.099, -0.080)	(0.048, -0.100, -0.077)	(0.048, -0.099, -0.077)
(θ_1, θ_2, θ_3, θ_4, θ_5) hardstop offsets (radians)	(0, 0, 0, 0, 0)	(-0.012, 0.004, -0.033, 0.028, -0.016)	(-0.010, 0.004, -0.029, 0.032, -0.039)
Link 1 (k_x, k_y, k_z) (N-m/rad)	(6106.9, 5892.0, 3922.7)	(6106.9, 5892.0, 3922.7)	(6106.9, 5892.0, 3922.7)
Link 2 (k_x, k_y, k_z) (N-m/rad)	(1871.5, 5887.2, 2761.9)	(1871.5, 5887.5, 2761.8)	(1871.5, 5887.5, 2761.8)
Link 3 (k_x, k_y, k_z) (N-m/rad)	(499.2, 780.7, 485.6)	(499.2, 780.7, 485.6)	(499.2, 780.7, 485.6)
Link 4 (k_x, k_y, k_z) (N-m/rad)	(3367.9, 1227.4, 322.2)	(3367.9, 1227.4, 322.2)	(3367.9, 1227.4, 322.2)
Link 5 (k_x, k_y, k_z) (N-m/rad)	(1112.5, 45438.0, 1024.7)	(1112.5, 45438.0, 1024.7)	(1112.5, 45438.0, 1024.7)

Table 2: IDD Calibration Parameters

It is interesting to note that in Table 2, the parameter estimation process tends to modify the D-H parameters and the joint offset values as opposed to modifying the stiffness parameters. In other words, the majority of the stiffness parameters in Table 2 did not vary from their initial, modeled values while most of the D-H parameters and joint offset values were updated through the least-squared error estimation process. From this result, the underlying sensitivity of the parameters as they related to the 3D position of the laser tracker targets mounted to the end of the IDD is assumed to be greater for the D-H and joint offset parameters when compared to the stiffness parameters. Finally, it is worth noting that the parameter estimation process described above subsumes any unmodeled effects (joint backlash, workmanship issues such non-orthogonal links, etc) into the parameters that have been modeled. It is not expected that the final parameter sets shown in Table 2 are representative of the real, as-measured IDD, but instead represent the best fit of the parameters to the model that relates IDD joint angles to end-effector or tool position.

Repeatability Performance

In addition to the kinematic and stiffness calibration process, the repeatability of the IDD was measured by moving the robot arm to specific poses within its workspace and measuring the laser tracker targets mounted to the IDD turret. A limited data set was captured for the Spirit IDD which resulted in a mean RSS position repeatability of 0.34 mm and 0.19 degrees in orientation. The mean plus 3σ RSS position repeatability is 0.42 mm and 0.25 degrees in orientation. A more extensive dataset was collected using the Engineering Model (EM) IDD and, for this arm, the resulting mean RSS position repeatability is 0.31 mm in position and 0.29 degrees in orientation while the mean plus 3σ RSS position error is 1.32 mm and 1.19 degrees in orientation. Recall that the system requirement for repeatability was specified to be 4 mm in position and 3 degrees in orientation. Clearly, the IDD exceeded this performance requirement by almost an order of magnitude for the mean position and orientation repeatability. The repeatability of the IDD turned out to be critical for certain surface operation functions as described in the next section.

As mentioned previously, the IDD was responsible for placing the *in situ* instruments on rover-mounted target (magnets and CCT) as well as stowing and deploying the IDD to and from the stow-for-drive position that is tucked under the front of the rover. To accomplish these positioning duties, a standard "teach-repeat" technique was utilized where, during ground testing, the desired instrument was precisely positioned relative to the rover-mounted target and the joint angles at this position were recorded. Since these teach points were learned under Earth gravity conditions, the deflection of the turret-mounted instruments will be different during nominal surface operations due to Martian gravity conditions. To account for this difference, the pose of the desired instrument is computed using the taught joint angles and the deflected kinematics described in Section 4. This taught pose is then used during Martian surface operations to command the desired instrument to the desired rover-mounted target. The deflection compensation technique described in Section 4 is utilized to compute the joint angles that achieve the desired end pose. These computed joint angles will certainly be different from the joint angles taught during Earth testing, however, the desired end pose will be the same on Mars as it was on the Earth.

The other related "teach-repeat" position set is associated with deploying the IDD from the stowed position under the rover and stowing it back to this position prior to rover mobility. The IDD deploy and stow operation consists of moving the IDD through a set of mostly single joint moves that maneuver the arm around and into various stow features mounted to the rover. Due to the changes in gravity conditions from when the deploy/stow sequence is taught to the IDD, the individual joint motions were modified by the expected droop of the IDD relative to the stow features when operating the IDD on the Martian surface.

The incremental positioning performance of the IDD is related to the minimum controllable motion that can be achieved by the IDD and closed-loop motion control system. A limited test was performed to validate this requirement and consisted of moving the MI relative to an optical distortion target. This target consisted of three square dot patterns of various spacing. The MI was moved

in 3 mm increments with respect to this optical target and MI images captured at each increment. Based on the motion of the dot patterns in the MI images and the known optical properties of the MI, the incremental motion of the IDD from image to image can be calculated. From a series of 5 such images, the mean incremental position change between images was computed to be 2.92 mm which can be compared to the commanded motion of 3 mm. As such, the IDD has the ability to control the incremental position of any instrument to much less than a millimeter.

Absolute Positioning Performance

For the absolute positioning requirement that includes both IDD positioning accuracy and front Hazcam stereo ranging accuracy, a limited number of ground tests were performed to evaluate this requirement specifically as it relates to the stereo ranging performance of the front Hazcam. However, during the rover system thermal test, the front Hazcams were required for producing targeting information for instrument placement activities within the thermal chamber since direct access was not possible. An IPS test fixture was located in the thermal chamber such that the fixture was positioned within the workvolume of the IDD. Mounted to the test fixture were two radiation sources for evaluating the MB and APXS instrument performance as a function of temperature and an optical distortion target that was used to evaluate MI positioning performance. The IPS test fixture included fiducials markings that allowed the 3D position and surface normals of the targets to be identified. From this information, IDD commands were generated for placement operations during this critical system thermal test.

During the Spirit system thermal test, it was noted that the positioning performance of the MI relative to the optical distortion target was not within the absolute positioning requirements (10 mm in position, 10 degrees in orientation). As a result of this test, the parameter estimation procedure described at the beginning of this section was re-visited and a bug was identified in the parameter estimation code. Specifically, a spacer that was used to mount the target tracking target bracket onto the IDD turret was not accounted for in the kinematics that computed the laser tracker target 3D position. A final set of instrument positioning tests were performed prior to final rover integration activities at Kennedy Space Center and confirmed that the IDD met the absolute positioning performance requirements.

A limited stereo ranging test was performed by placing the IPS test fixture within the workvolume of the IDD and surveying the test fixture itself and fiducials on the test fixture with respect to the rover coordinate frame. From this single data set, the 3D stereo ranging performance was computed by comparing the surveyed points to the stereo solution for these points. For the six points evaluated, the mean RSS error was 3.9 mm in position while the mean plus 3σ RSS position error was 7.66 mm. When combining this result with the IDD positioning accuracy numbers using an RSS approach, the overall absolute positioning performance for the Spirit rover yields a mean RSS position error of 4.26 mm and mean plus 3σ RSS position error of 9.61 mm. For the Opportunity rover, the mean RSS position error is 4.12 mm and the mean plus 3σ RSS position error is 8.45 mm. For the evaluation of the absolute orientation performance of the combined IDD and stereo front Hazcam system, only qualitative tests were performed to validate this requirement.

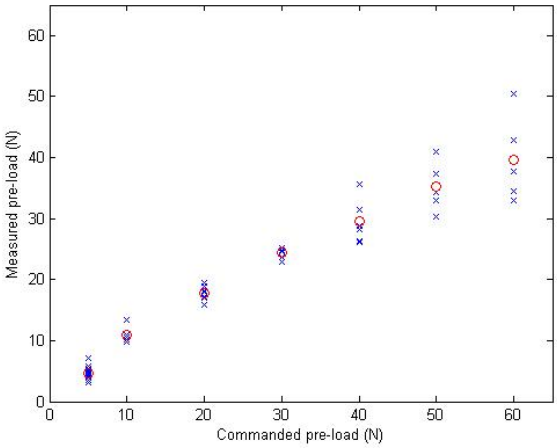

Figure 15: Measured vs. Commanded Preload

Preload Performance

As discussed in Section 4, the stiffness model of the IDD along with the IDD and instrument mass properties are utilized to determine the commanded overdrive of the arm that corresponds to a required preload force that an instrument exerts on a hard target assuming that the instrument is in contact with the hard target. To validate the ability of the stiffness model to accurately predict the commanded preload force, a series of tests were performed that positioned the IDD in seven different poses and measured the actual preload force using a single axis force sensor mounted to the IPS test fixture. A number of commanded preloads were then executed at each pose and compared to the measured preload. Figure 15 shows a plot of the commanded versus measured preload for the seven pose configurations of the IDD with the mean measured preload preload shown in the plot by the red circle.

As shown in Figure 15, the measured preload is generally smaller than the commanded preload. For low commanded preload values (<30N), the stiffness model does an adequate job for the tested pose configurations and the correspondence between the commanded preload and measured preload is quite good with a low standard deviation for the error between the commanded and measured preloads (~1N). As the commanded preload is increased, the predictive ability of the stiffness model deteriorates and both an underestimation of actual applied

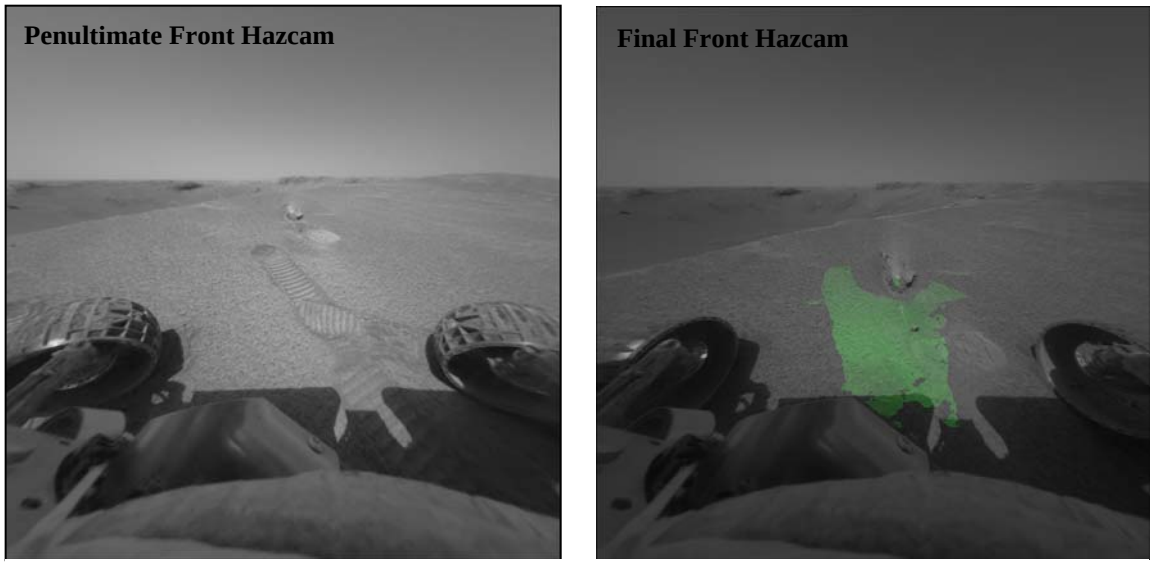

Figure 16: Penulatimate and final front Hazcam images and associated Reachability Map

preload and a growth in the uncertainty of the applied preload is experienced.

6. SURFACE OPERATIONS HIGHLIGHTS

In this section, the primary process for operating the IDD and associated *in situ* instruments is described along with some representative results from Martian surface operations. The surface operation of the IDD starts with the acquisition of a set of front Hazcam stereo image pairs. Typically, two stereo pairs are acquired with the first designated as the penultimate Hazcam and the second designated as the final Hazcam with 50-80 cm of rover motion separating the two image pairs. Two images are acquired since the entire deployment volume of the IDD as it moves out of its stow position is not completely visible in the final front Hazcam image. The penultimate image pair serves as a means to check what is under the rover in the final position and to validate that the deploy volume is clear of any objects that would interfere with the IDD deployment. Representative penultimate and final front Hazcam stereo images from the Opportunity rover outside of Endurance crater are shown in Figure 16.

When the final front Hazcam stereo image pair is transmitted from the rover to Earth, a data processing pipeline operates on the image pair in order to generate stereo range data relative to the rover reference frame. From this generated range map, a number of products are derived including a surface normal map which is computed by fitting (in a least-squared error sense) a plane to the cloud of range points surrounding a valid point in the stereo range map. From the combined range map and surface normal map, a ground version of the IDD flight software is utilized to test the ability of the IDD to reach out and place each one of the *in situ* instruments on the valid range and surface normal points. This so-called "reachability" map is then used to select targets for science instrument placement activities. The computation of the reachability map includes testing the four major configurations of the IDD (elbow up and wrist up, elbow down and wrist up, elbow up and wrist down, and elbow down and wrist down) as well as predicted collisions between the IDD, the instruments, the rover, and the terrain using the collision detection algorithm described in Section 4. A representative reachability map from the Opportunity rover is shown in the right image in Figure 16 and the subsequence placement of the APXS instrument on this rock is shown in Figure 17.

As discussed previously, the repeatability performance of the IDD has been extremely important during nominal

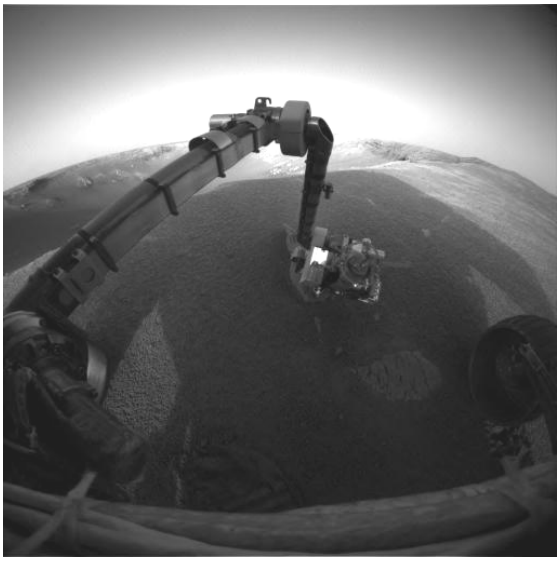

Figure 17: APXS placement

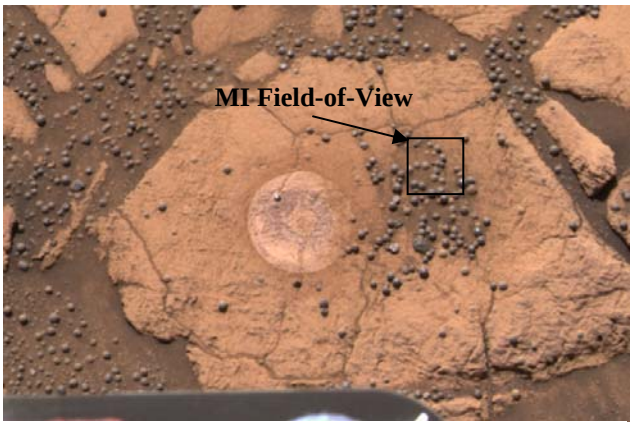

Figure 18: Pancam Image of the Berry Bowl

surface operations. The ability to place one instrument on a rock or soil target and then place a second instrument on the same science target with a repeatability of 1 mm in position and 1 degree in orientation. During the Opportunity rover's surface operations within Eagle Crater, there was a very strong desire by the science team to identify the chemical composition of the small "blueberries" or spherules that were located throughout the crater. The spherules are 3 mm in diameter and, therefore, are too small to target directly using the front Hazcam. The Opportunity rover approached a location in Eagle Crater known as the "Berry Bowl" where a significant number of spherules had collected. A Pancam image of the Berry Bowl is shown in Figure 18.

The IDD was commanded to maneuver the MI over a portion of the Berrry Bowl that was thought to contain a high concentration of spherules. A series of MI images were taken over this area and downlinked to the ground. The ultimate objective was associated with the placement of the MB spectrometer on a cluster of spherules to determine the iron chemistry of these unique geologic features. Within the field of view of the MI, a cluster of spherules was identified to be targeted for the MB placement. This targeting is shown in the left image of Figure 19. The known image resolution of the MI (32 microns per pixel) was then used to compute the horizontal and vertical offsets relative to the center of the MI image. On the next uplink cycle, the MB was placed at the same location where the MI targeting image was acquired and then the horizontal and vertical offsets were commanded as a relative tool-frame Cartesian motion. The MB was then driven down onto the surface. On the subsequent sol, the MB was removed from the target and another MI image was captured to document the MB placement. This image is shown in the right portion of Figure 19 along with the associated MI field-of-view in the Pancam image in Figure 18. Comparing the center pixel of the MI image to the targeted pixel and applying the image resolution yields an absolute positioning performance of 0.8 mm. The resulting MB spectrum revealed that the spherules were comprised of the mineral hematite which helped to explain the orbital data that indicted that Meridiani Planum was rich in grey hematite. In addition to identifying the source of the hematite, the *in situ* instruments also detailed the fine scale rock formations that are associated with liquid water wave actions and the detailed geochemistry that pointed to a sulfer-rich ocean at Opportunity's landing site. Finally, this single ground cycle "eye-in-hand" technique has been utilized operationally multiple times to significantly increase the absolute positioning performance of the IPS by an order of magnitude (from 10 mm down to 1 mm).

In summary, the MER Instrument Positioning System has performed flawlessly during numerous deploy/stow cycles and has carried out many *in situ* observations while deployed. While a full accounting of the number of

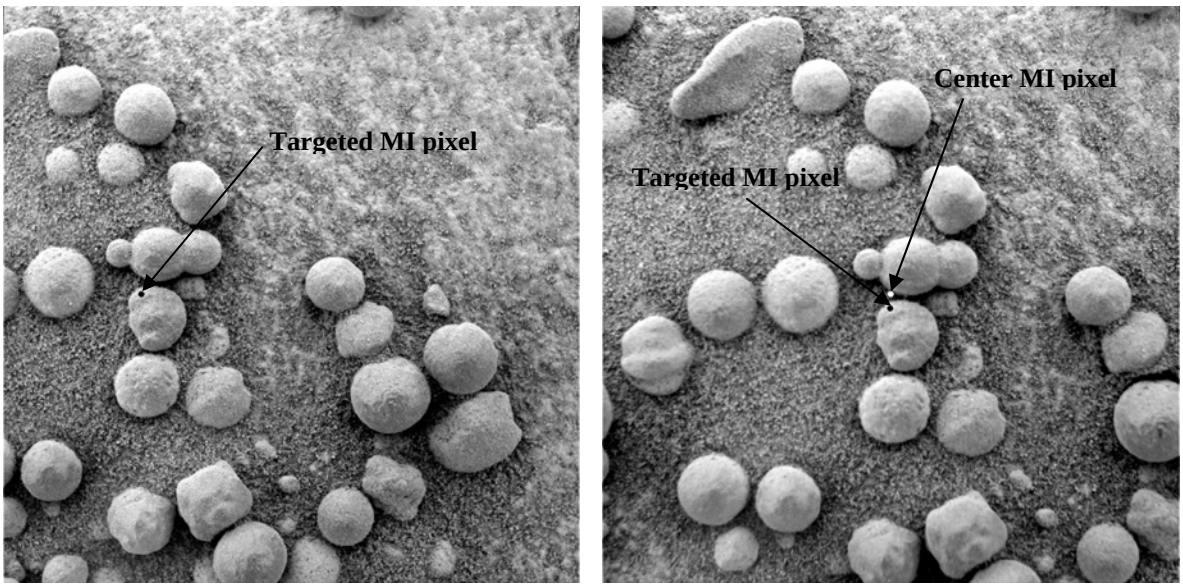

Figure 19: MI Images of Berry Bowl Spherules

deploy/stow cycles and science observations per rover has not been performed, a tally has been made for the Opportunity rover at the end of its prime mission (90 sols on Mars). By sol 90, the IDD had been deployed and stowed 36 times, acquired 43 APXS measurements, acquired 89 MB spectrometer measurements, acquired 766 MI images, and performed 8 RAT grind activities. At the time of writing, the IDD mechanism has successfully completed all commanded operations on both Spirit and Opportunity totaling over a combined 600 sols on the surface or Mars.

7. CONCLUSIONS

This paper has described in detail the Mars Exploration Rover's Instrument Positioning System and the use of this sub-system to carryout *in situ* operations of the Martian surface and sub-surface. All told, the IDD has served as an exceptional robotic mechanism for performing robust and reliable *in situ* science. The ability to carry out high precision mobile manipulation functions provided by the rover and the IDD has been critical to the understanding of the water processes at both the Spirit and Opportunity landing sites. As such, the Mars Exploration Rover's Instrument Positioning System has paved the way for the use of future robotic devices that advance NASA's capabilities in autonomous manipulation, sample acquisition, and *in situ* science investigations.

ACKNOWLEDGMENTS

The research described in this paper was carried out at the Jet Propulsion Laboratory, California Institute of Technology, under a contract with the National Aeronautics and Space Administration.

REFERENCES

[1] S. W. Squyres, et al., "Athena Mars Rover Science Investigation," *Journal of Geophysical Research*, *108*(E12), 8062, doi:10.1029/2003JE002121, 2003.

[2] G. Klingelhöfer, et al., "Athena MIMOS II Mössbauer Spectrometer Investigation," *Journal of Geophysical Research*, *108*(E12), 8067, doi:10.1029/2003JE00 2138, 2003.

[3] R. Rieder, et al., "The New Athena Alpha Particle X-ray Spectrometer for the Mars Exploration Rovers, *Journal of Geophysical Research, 108*(E12), 8066, doi:10.1029/2003JE002150, 2003.

[4] K. E. Herkenhoff, et al., Athena Microscopic Imager Investigation, *Journal of Geophysical Research*, *108*(E12), 8065, doi:10.1029/2003JE002076, 2003.

[5] S. P. Gorevan, et al., "Rock Abrasion Tool: Mars Exploration Rover Mission," *Journal of Geophysical Research*, *108*(E12), 8068, doi:10.1029/2003JE00 2061, 2003.

[6] R. Fleischner, "Concurrent Actuator Development for the Mars Exploration Rover Instrument Deployment Device," *Proceedings of the 10th European Space Mechanisms and Tribology Symposium*, San Sebastian, Spain, September 2003.

[7] S. P. Dougherty, "Micro-Imager Dust Cover, Micro-Imager Contact Sensor, and Mössbauer Spectrometer Contact Sensor Mechanisms for the Mars Exploration Rovers," *Proceedings of the 10th European Space Mechanisms and Tribology Symposium*, San Sebastian, Spain, September 2003.

[8] M. W. Spong and M. Vidyasagar, *Robot Dynamics and Control*, John Wiley and Sons, Inc., New York, 1989.

[9] Taylor, R., "Planning and Execution of Straight-line Manipulator Trajectories", IBM Journal of Research and Development, Vol. 23, No. 4, pp. 424-436, 1979

[10] C. Leger, "Efficient Sensor/Model Based On-Line Collision Detection for Planetary Manipulators," *Proceedings of the 2002 IEEE International Conference on Robotics and Automation*, pp. 1697-1703, May 2002.

[11] S. Gottschalk, M. C. Lin and D. Manoch, *OBB-Tree: A hierarchical Structure for Rapid Interference Detection.* Technical Report TR96-013, Department of Computer Science, University of North Carolina, Chapel Hill, 1996.

BIOGRAPHIES

Eric T. Baumgartner is a Senior Engineer and Supervisor of the Mechanical and Robotic Technologies Group at the Jet Propulsion Laboratory. During the Mars Exploration Rover project, he served as the lead systems, test and operations engineer for the Instrument Positioning System. He currently leads the development of the robot arm and sampling system for the 2009 Mars Science Laboratory flight mission. Dr. Baumgartner received the Ph.D. degree in Mechanical Engineering from the University of Notre Dame in 1992 and his research interests include the use of vision for precision manipulation and sensor fusion techniques for rover localization.

Robert G. Bonitz is with the Telerobotics Research and Applications Group at the Jet Propulsion Laboratory where he is currently the Phoenix Lander 2007 Robotic Arm Manager. Previously he developed the control algorithms and software for the Mars Exploration Rover and Mars Polar Lander robotic arms. He has conducted research in control algorithms for multiple-manipulator robotic systems, robust internal force-based impedance controllers, frameworks for general force decomposition, optimal force control algorithms, and calibration methods for multi-arm robotic systems. He has worked for a variety of industrial companies including Raytheon, TRW, Source 2 International, and GTE. He has a Ph.D. in Electrical Engineering from the University of California, Davis.

Joseph P. Melko is with the Advanced Mechanical Systems group at the Jet Propulsion Laboratory where he is currently the Mechanisms Operation Lead on the Mars Exploration Rover Project (MER). During the development and production phase of MER, he was the Mechanical System Engineer for the rover element and Technical Lead for the rover mechanical payloads. He previously worked in the Sensors and Mechanisms Department at Hughes Space & Communications, developing and delivering a variety of flight mechanisms. He has an MS in Mechanical Engineering and BS in Aerospace Engineering, both from the University of California, Los Angeles.

Lori R. Shiraishi is with the Advanced Mechanical Systems Group at the Jet Propulsion Laboratory where she is currently the Phoenix Lander 2007 Robotic Arm Mechanical Cognizant Engineer. She has been with JPL since 1988 and has served as Cognizant Engineer on a variety of spacecraft and instrument electromechanical devices, including the Mars Exploration Rover Instrument Deployment Device, Tropospheric Emissions Spectro-meter Translator Assembly, Cassini Main Engine Assembly Cover, Cassini Visible and Infrared Mapping Spectrometer Cooler and Cover Release System, and Hinge-line Mechanisms for the Spaceborne Imaging Radar, Version C. She has a BS in Mechanical Engineering from the University of California, Berkeley.

P. Chris Leger is with the Jet Propulsion Laboratory's Mechanical and Robotic Technologies Group, where he is currently a Rover Planner for the Mars Exploration Rovers. He also developed flight software for the rovers' entry, descent, and landing system, as well as rover mechanical hardware and rover simulation and data analysis software. Before MER, he performed research in rover hazard avoidance, inflatable rover design and optimization, and rover operation methods. Previously he worked on Darwin2K, and automated synthesis and optimization package for robot configuration design, and 3D computer vision and hazard avoidance for the Autonomous Loading System, an automated commercial excavator. He has a Ph.D. in robotics from Carnegie Mellon University.